Evaluation of Fracture Behavior of SA-516 Steel Welds Using Acoustic Emission Analysis

Eui Gyun Na*
Mechanical Department of Engineering College, Kunsan National University, San 68, Miryong-Dong, Kunsan, Chonbuk 573-701, Korea
Kanji Ono
Department of Materials Science and Engineering, University of California, Los Angeles, CA, U.S.A
Dong Whan Lee
Mechanical Department of Engineering College, Chonbuk National University, Jeonju-Si, Jeonbuk 561-756, Korea

The purpose of this study is to evaluate the AE characteristics for the basemetal, PWHT (post-weld heat treatment) and weldment specimens of SA-516 steel during fracture testing. Four-point bending and AE tests were conducted simultaneously. AE signals were emitted in the process of plastic deformation. AE signal strength and amplitude of the weldment was the strongest, followed by PWHT specimen and basemetal. More AE signals were emitted from the weldment samples because of the oxides, and discontinuous mechanical properties. AE signal strength and amplitude for the basemetal or PWHT specimen decreased remarkably compared to the weldment because of lower strength. Pre-cracked specimens emitted even lower event counts than the corresponding blunt notched specimens. Dimple fracture from void coalescence mechanism is associated with low-level AE signal strength for the basemetal or PWHT. Tearing mode and dimple formation were shown on the fracture surfaces of the weldment, but only a small fraction produced detectable AE.

Key Words: AE Signals, Events, Signal Strength, Amplitude, Plastic Deformation, Dimple Fracture, Tearing, Oxides

1. Introduction

AE technique is a useful tool for the study of elastic-plastic deformation behavior, fracture monitoring, detection of crack initiation and fracture mechanisms for the metals, composites, and structures in field (Ono et al., 1984 ; Nakamura et al., 1980). However, few papers related with the weldment and AE technique were published in domestic and foreign countries (Mukherjee et al., 1997 : Roberts et al., 2003 : Na et al., 2002). Besides, those papers don't have the contents related with the way how to eliminate the noises such as mechanical and electrical ones which were introduced in the process of experiment necessarily. So, it is meaningful to show the procedure to eliminate the noises and to distinguish the real AE signals and noises through the analysis of AE events distribution after test. On the other hand, most fracture for the structures in industrial fields is initiated at welded region because there are high possibilities to contain defects such as porosity, oxides and incomplete penetration at welds. Accordingly, in order to

* Corresponding Author,
E-mail : egna@kunsan.ac.kr
TEL : +82-63-469-4719; **FAX** : +82-63-469-4727
Mechanical Department of Engineering College, Kunsan National University, San 68, Miryong-Dong, Kunsan, Chonbuk 573-701, Korea. (Manuscript **Received** June 1, 2005; **Revised** December 23, 2005)

prevent an abrupt failure of the weld structures, it is necessary to evaluate AE characteristics and fracture mechanisms of the welded region in the process of deformation and fracture.

The purpose of the of this study is to show the way how to eliminate the noises through the analysis of AE events distribution, to investigate the differences AE characteristics between the blunt notched and pre-cracked basemetal, weldment and PWHT specimens. Finally, SEM observations were made to find out the fracture mechanism.

2. Experimental Apparatus and Method

2.1 Material and welding

The material used in this study is an SA516 steel plate of 38-mm thickness. Table 1 shows the chemical compositions and mechanical properties at room temperature. Submerged-arc welding with 3 passes was conducted along the rolling direction. Table 2 represents the welding conditions. PWHT was conducted under the following conditions : heating rate of 145℃/hr, heating temperature of 630℃ and holding time of 100 min. Standard Charpy V-notch (45°) specimens were machined from the weld zones and basemetal.

Table 1 Chemical compositions and mechanical properties

(a) Chemical compositions (wt.%)

C	Si	Mn	P	S	Cr	Ni	Cu	V	Sol Al
0.21	0.237	1.06	0.016	0.004	0.02	0.02	0.02	0.012	0.26

(b) Mechanical properties

Yield strength (MPa)	Tensile strength (MPa)	Elongation (%)
358.7	519.5	29.0

Table 2 Welding conditions

Pass	Amphere (A)	Voltage (V)	Traveling speed (cm/min)
1st	200	24	37
2nd	300	28	30
3rd	550	30	30

Figure 1 represents the details of an extraction of the specimen from the welded and heat treated blocks. Fusion line is centered on the specimens.

Figure 2 represents the load and deflection for the basemetal, PWHT specimen and weldment. Elastic modulus at elastic region is almost same and strength of the weldment at constant plastic deflection was highest, followed by PWHT specimen and basemetal.

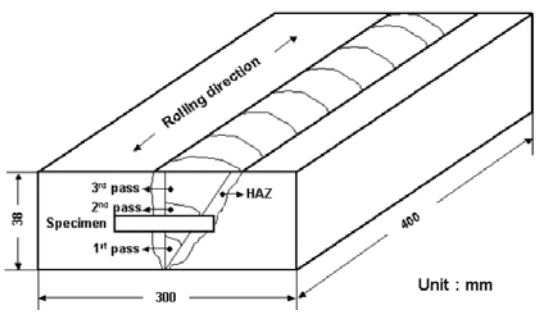

Fig. 1 Extraction of specimen from the welded block

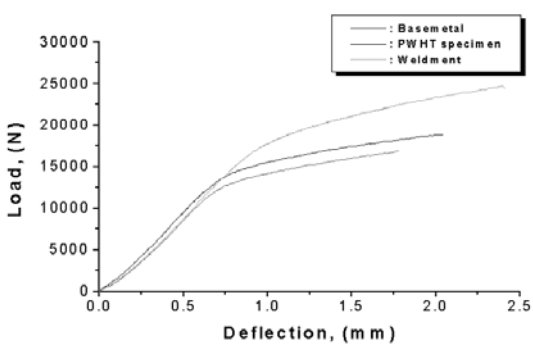

Fig. 2 Relationship of load and deflection for the basemetal, PWHT specimen and weldment

2.2 Experimental method

Figure 3 shows the schematic diagram of mechanical and AE tests. Four-point bend test was conducted at a constant speed of 0.05 mm/min at room temperature. Span length was 40 mm and the top-loading span was 10 mm. AE measurements were obtained using two AE sensors (PAC-R15) and preamplifiers (PAC-1220A, 40 dB gain). Two transducers were coupled to both end of the Charpy specimen. One sensor was attached with a 20-mm insert to shift the AE

location from the dead center. Threshold value was 40 dB for both the blunt notched and pre-cracked specimens. The AE parameters were AE events, signal strength, energy, counts, rise-time and amplitude distribution of AE signals. AE signal analysis was conducted using AE Win software, which was set up to detect the AE signals only from the notch region.

In order to eliminate the noise from loading pins, only AE waves, which arrived within 10 μs to both channels were chosen for analysis. Further discrimination was conducted based on the event location. Among AE waves thus discriminated, AE waves, which differ in rise-time of >3 μs, were ignored. Short duration pulses of electrical nature were detected often, but were thrown away through count and rise-time filtering.

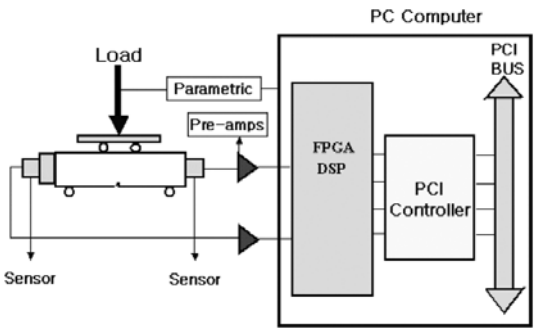

Fig. 3 Schematic diagram for experimental set-up under 4 point bending test

3. Results and Discussion

3.1 Blunt notched and pre-cracked specimens

Figure 4 shows AE event distributions along the specimen length for the blunt notched basemetal, PWHT specimen and weldment, which

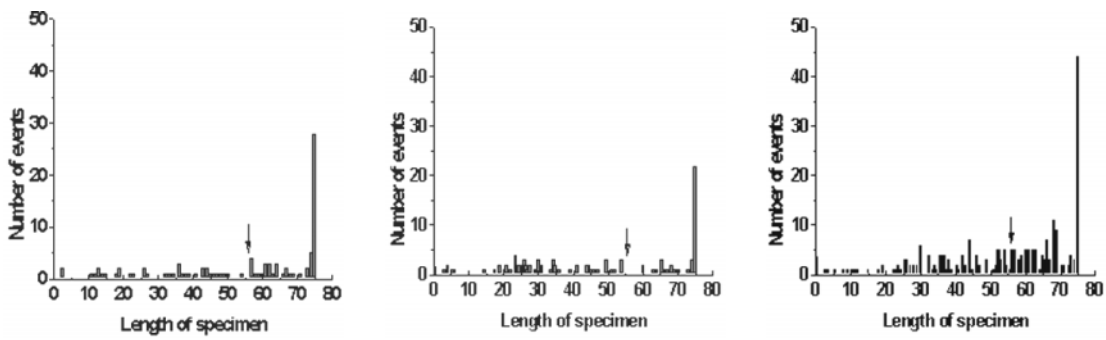

(a) Basemetal (b) PWHT specimen (c) Weldment

Fig. 4 Event distributions during AE test (Arrow shows notch position)

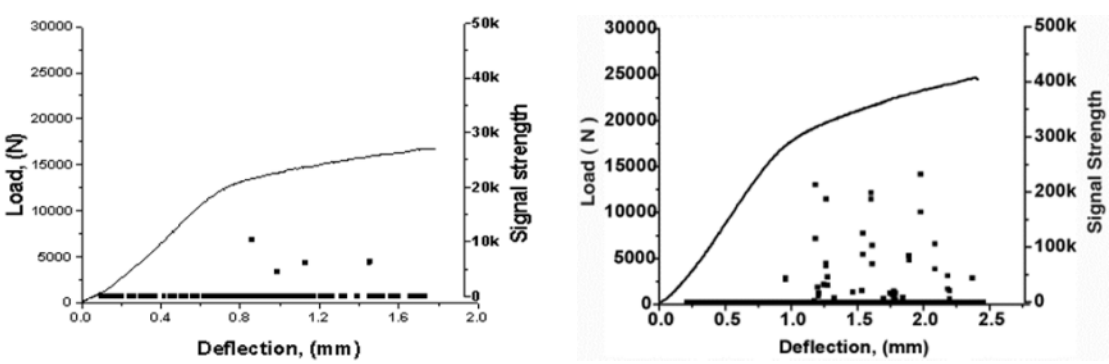

(a) Basemetal (b) Weldment

Fig. 5 Load and AE signal strength plotted against deflection for the blunt notched samples

were obtained using a linear location graph. Among total AE events, AE events that were produced around the notch (calibrated at 56 mm position) can be classified as effective AE events.

Figure 5 represents the load and deflection curves for the basemetal and weldment, including signal strength of AE waves from the notch region. Tests were terminated at maximum load. In all cases, AE signals were almost completely absent within the elastic region and a small number of signals were produced in the process of plastic deformation. The weldment specimen was the most active over the whole plastic deformation region with 27, whereas the basemetal showed only 4 events.

Figure 6 illustrates the AE counts vs. amplitude plots for the basemetal, PWHT specimen and weldment. Amplitude ranges are 43–56 dB for the basemetal, 43–65 dB for the PWHT specimen and 45–75 dB for the weldment.

Figure 7 shows the load and AE data for the fatigue pre-cracked specimens, including AE signal strength. Regardless of the basemetal and weldment, the pre-cracked specimens generated lower number numbers of AE signals and lower signal strength over the whole deflection range compared with those of the blunt notched specimens.

3.2 AE characteristics

Table 3 summarizes the AE properties for the blunt notched and pre-cracked specimens. In case of the blunt notched specimens, the maximum signal strength of the basemetal, PWHT specimen and weldment increased in order and the maximum amplitude values also changed from 56 to 75 dB. In case of the pre-cracked specimens, both of these values decreased. The maximum signal strength for the basemetal, PWHT specimen and weldment varied from 10,244 to 154,845 and the maximum amplitude values changed 51 to 68 dB. The results clearly indicate that the pre-cracked specimens emitted lower AE signals than the corresponding blunt notched specimens. This is ex-

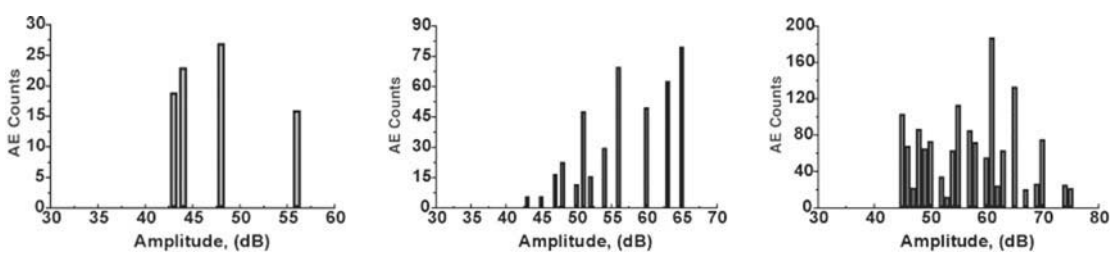

(a) Basemetal (b) PWHT specimen (c) Weldment

Fig. 6 AE counts vs. amplitude distribution

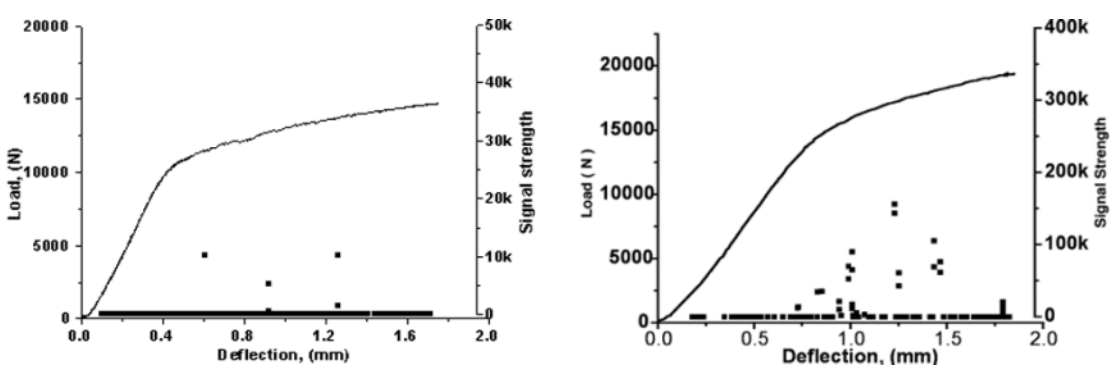

(a) Basemetal (b) Weldment

Fig. 7 Load and AE signal strength plotted against deflection for the pre-cracked PWHT specimen and weldment

Table 3 AE properties for notched specimens

(a) Blunt notched specimen

	Basemetal	PWHT	Weldment
No. of effective AE events	4	9	27
Max.strength	14,344	102,689	236,414
Max. amp	56	65	75
Total counts	96	454	1,451

(b) Pre-cracked specimen

	Basemetal	PWHT	Weldment
No. of effective AE events	3	6	17
Max.strength	10,244	84,593	154,845
Max. amp	56	65	75
Total counts	76	387	757

pected because pre-cracked specimens have smaller plastic zones at the crack tip compared with the blunt notched specimens because of lower load levels. The fracture process zone is also smaller (Leslie, 1983)

Figure 8 represents the relationship between signal strength and specimens for the blunt notched and pre-cracked specimen. Regardless of the blunt notched and pre-cracked specimens, signal strength of the weldment was the highest, followed by PWHT specimen and basemetal. In addition, signal strength of the pre-cracked specimens was lower than that of the blunt notched specimens. From these results, we found out the facts that signal strength of the specimens has close relations with the material strength and that of specimens depends on the specimen shape.

Figure 9 represents the SEM photos of the notch-tip region of the blunt notched basemetal,

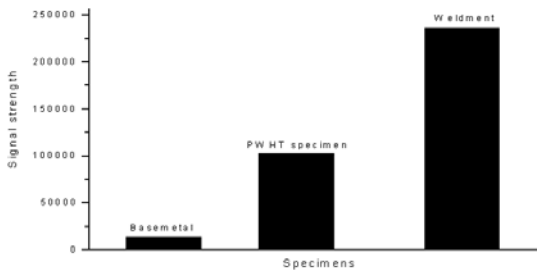

(a) Blunt notched specimens

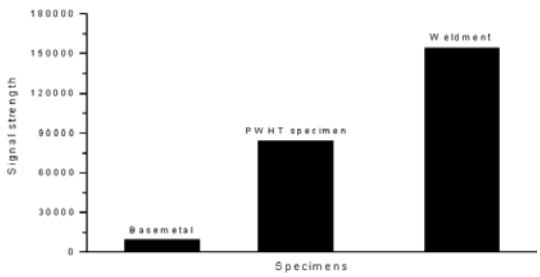

(b) Pre-cracked specimens

Fig. 8 Relationship between signal strength and specimens for the blunt notched and pre-cracked specimens

PWHT specimen and weldment, which were loaded midway between general yield and maximum load, and then unloading. The samples did not indicate the presence of a crack via the liquid penetrant inspection. However, these were examined by SEM.

In the basemetal sample, a large fraction of the notch tip had dimple fracture area (A) ahead of the notch (N) and a few secondary cracks (B) can be seen. The dimple cracks are less than 30 μm deep and 60-100 μm wide. Individual dimples are small, typically a few μm in diameter. Some

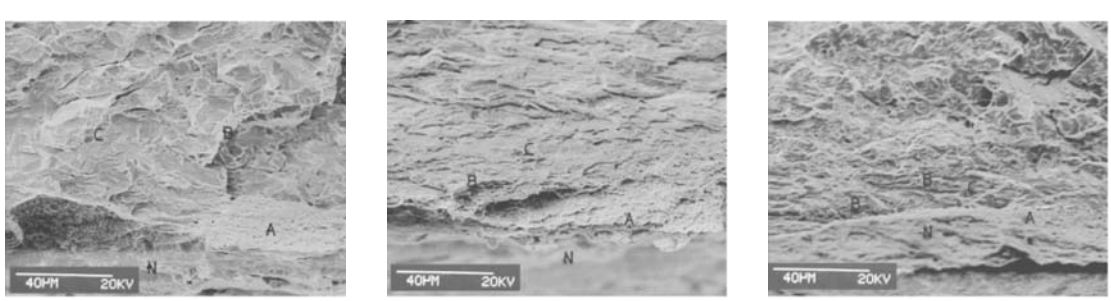

(a) Basemetal (b) PWHT (c) Weldment

Fig. 9 SEM fractograph for the blunt notched specimens

isolated voids around an inclusion are also found (C). Most of the rest is covered by the cleavage fracture surfaces. Since the width of the Charpy specimen was 10 mm, 50-100 distinct areas of dimple crack (as marked by A in Figure 9(a)) are present. In the PWHT specimen, dimple fracture areas (A) and void around inclusion (C) ahead of the notch tip were found along with a few secondary cracks (B). In this case, the dimple cracks are larger and their number is 30-60. In both cases, however, we cannot rule out the secondary cracks due to the cryo-cracking. In the weldment, dimple crack (A) as well as many secondary cracks near the notch (B) were found. These secondary cracks appear to be initiated at oxides which are formed during welding process. These were produced over the whole region and have different crack morphology from those found near dimple cracks in Figure 9(a) and 9 (b). Both dimple cracks and secondary cracks are estimated to amount to about 50 across the specimen.

Figure 10 shows the SEM photos of the pre-cracked specimens, which were taken after loading. The load level was the mid-point between yield and the maximum load. In case of the basemetal, regions of small dimples (A) and void (B) ahead of the notch (N) can be seen. The area near mark (N) shows fatigue crack. Some secondary cracks were shown near the pre-cracked region (C), while cleavage area is marked (D). However, fracture surfaces for the weldment were quite different. A well-developed stretch zone (A) extends ahead of the pre-cracked tip (N). Similar tearing dimples (A) are found elsewhere (left and right of mark C), and irregular dimples (B) and large secondary cracks can be seen unlike the basemetal. Some of the secondary cracks are associated with microstructural features and appear to follow the grain boundaries.

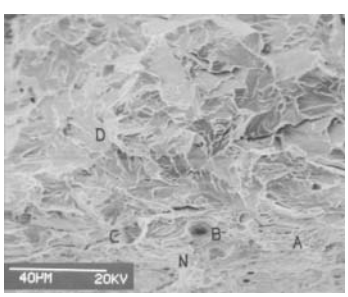

(a) Basemetal

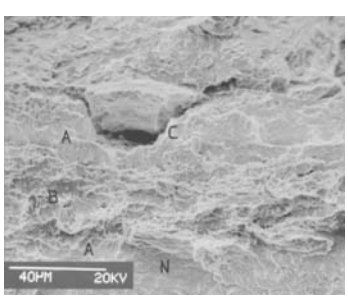

(b) Weldment

Fig. 10 SEM fractographs for the pre-cracked specimens

3.3 AE mechanisms

Fractographic examination indicates that microcracks are initiated at loading between the yield and the midway point to the maximum load. AE signals are generated at the same loading range. Thus, AE generation can be used as the crack initiation indicator. However, this does not imply that the AE signals observed correspond to microcracking. Since we need to use high sensitivity sensor to detect the signals, we cannot rely on the waveform and spectral information to positively identify the signal origin. Next, the number of AE events, especially in the basemetal and PWHT samples, is small and spurious signals are distributed over the length of the sample as shown in Figure 4. Accordingly, the source location by itself does not ensure the AE signals which come from cracking at the notch position. Thirdly, the number of dimple cracks are found in the basemetal and PWHT specimen. These dimple cracks attributed to generate only weak emission (Ono et al., 1984).

The stronger AE signal strength, amplitude and more AE event counts for the weldment are expected. The microstructure of the weldment is comprised of untempered and partially tempered martensite, and has more coarse grain structures as shown in Figure 11. It is also heterogeneous because some parts are heated during multi-pass welding. In addition, some oxides and porosities

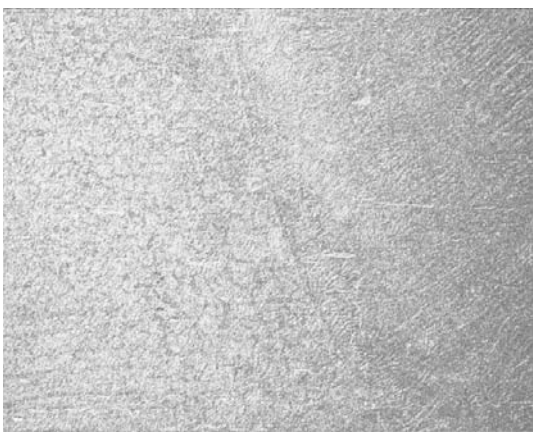

Fig. 11 Microstructures of the welded region

are inevitably formed even under the submerged-arc welding condition. These factors may cause to emit AE with the larger signal strength and higher peak amplitude. Fractographic evidence for oxide debonding and porosity-induced emission is yet to be uncovered, but the previous section demonstrates that secondary cracks from hard-phase separation (C in Figure 10(b)) exist. Secondary cracks at the notch-root (B in Figure 9(c)) should also contribute to AE in blunt notched samples. These are sources of some of the observed AE in the weldment.

The mode of plastic deformation at the notch-tip can be another factor. According to the past study (Na, 1983), the shape of plastic deformation at notch tip of the weldment spreads out perpendicular to the notch direction, whereas that of the basemetal and PWHT specimens proceeds to the notch direction, even though plastic deformation size at notch direction of the weldment becomes smaller. This was evident in the sample loaded to the maximum load. Macro-cracks in weldmentl samples started to spread along the expected shear bands. More AE signals are emitted due to the increased area of cracking. In the weldment, residual stresses must be considered as an extra factor. However, residual stresses are removed in the process of machining the Charpy-sized specimens. So, effects of residual stresses on AE activity can be ignored in the present case.

AE signal strength and peak amplitude for the PWHT specimen decreased remarkably compared with the weldment. The matrix of the PWHT specimen becomes softer than that of the weldment. So, the plastic zone grows easily and only emissions of rather low amplitude are produced.

4. Conclusions

AE from the fracture of weldment was examined using modern instrumentation. The findings are summarized below.

(1) Pre-cracked and blunt notched specimens emitted low event counts, weak signal strength and low peak amplitude in basemetal and PWHT specimens. The stronger AE signal strength, amplitude and more AE event counts for the weldment were found in both types of specimen.

(2) AE signals are generated at load between the yield and the midway point to the maximum load, in which microcracks are initiated. Thus, AE generation can be used as the crack initiation indicator.

(3) Observed AE signal strength and amplitude in the basemetal and PWHT specimens are unlikely to result from dimple cracking shown in these samples. However, tearing fracture and formation of large secondary cracks observed in the weldment possibly cause the strong signal strength and high amplitude in the weldment.

Acknowledgments

This work was financially supported by the Kunsan National University's Long-term Overseas Research Program for Faculty Member in the year 2004. One of the authors gratefully acknowledges the financial support by Kunsan National University. We appreciate a valuable comment by Allen T. Green at AEWG47 regarding the source location scheme.

References

Leslie, W. C., 1983, Iron Steel Soc. AIME Trans. 2, pp. 1～24.

Mukherjee, P. and Barat, P., 1997, "Acoustic

Emission Studies on Welded and Thermally Treated AISI 304 Stainless Steel during Tensile Deformation," *Scripta Materialia*, Vol. 37, No. 8, Elsevier Science, pp. 1193～1198.

Na, E. G., You, H. S. and Kim, H., 2001, "Study on Characteristics of SCC and AE Signals for Weld HAZ of HT-60 Steel," *Journal of the Korean Society for Non-destructive Testing*, Vol. 21, No. 1, pp. 62～68.

Na, E. G., 1983, "Effect of PWHT on Fracture Toughness at Weld HAZ for Cr-Mo Steel," Master Thesis, Jeonbuk National Univ..

Nakamura, N., Ringshall, N., Fukuzawa, Y. and Adachi, A., 1980, "Acoustic Emission during the Deformation of Iron Crystals," *Proc. of the 5th International Acoustic Emission Symposium*, pp. 318～325.

Ono, K., Teoh, H. B. and Roman, I., 1984, "Fracture Induced Acoustic Emission of A533B Steel — Effects of Test Temperature and Fracture Mechanisms," *Progress in Acoustic Emission II*, pp. 105～113.

Roberts, T. M. and Talezadeh, M., 2003, "Acoustic Emission Montoring of Fatigue Crack Propagation," *Journal of Constructional Steel Research 59*, Elsevier Science, pp. 695～712.